Electronic Supplementary Material (ESI) for Journal of Materials Chemistry A.
This journal is © The Royal Society of Chemistry 2020

Supporting Information

Suppressing ice growth by integrating the dual characteristics of antifreeze proteins into biomimetic two-dimensional graphene derivatives

Xing Liu[1], Hongya Geng[2], Nan Sheng[3,4], Jianjun Wang[5], Guosheng Shi[1,4]*

[1]Shanghai Applied Radiation Institute and State Key Lab. Advanced Special Steel, Shanghai University, Shanghai 200444

[2]Department of Materials Imperial College London Prince Consort Road, London SW7 2AZ, UK

[3]Department of Physics, East China University of Science and Technology, Shanghai 200237, China

[4]Division of Interfacial Water, CAS Key Laboratory of Interfacial Physics and Technology, Shanghai Institute of Applied Physics, Chinese Academy of Sciences, Shanghai 201800

[5]Key Laboratory for Green Printing, Beijing National Laboratory for Molecular Science, Institute of Chemistry, Chinese Academy of Sciences, Beijing 100190

**Corresponding author. E-mail: gsshi@shu.edu.cn (G.S.)*

Context:

PS1. Different functional-group-modified graphene derivatives in simulation calculations

PS2. Autocorrelation function of hydrogen bonds between the hydroxyl on the two sides of GR–CH_3–OH–Mimic and ice or water

PS3. Distribution of the tetrahedral order parameter $P(q_t)$ for trapped water molecules on both sides of GR–CH_3–OH–Mimic

PS4. Radial distribution function of water molecules on two sides of GR–CH_3–OH–Mimic

PS5. Growth rate of ice crystals in different systems from theoretical calculations

PS6. The method to calculate lifetime of trapped water molecules and dynamic properties of hydration water on the two sides of GR–CH_3–OH–Mimic

PS7. The effect of GR–NH_2–OH–Mimic on ice growth

PS8. The snapshot of trapped water on both sides of GR–OH–O–Mimic

PS9. Details of experimental growth rates of ice crystals in the presence of different functional-group-modified graphene

PS1. Different functional-group-modified graphene derivatives in simulation calculations

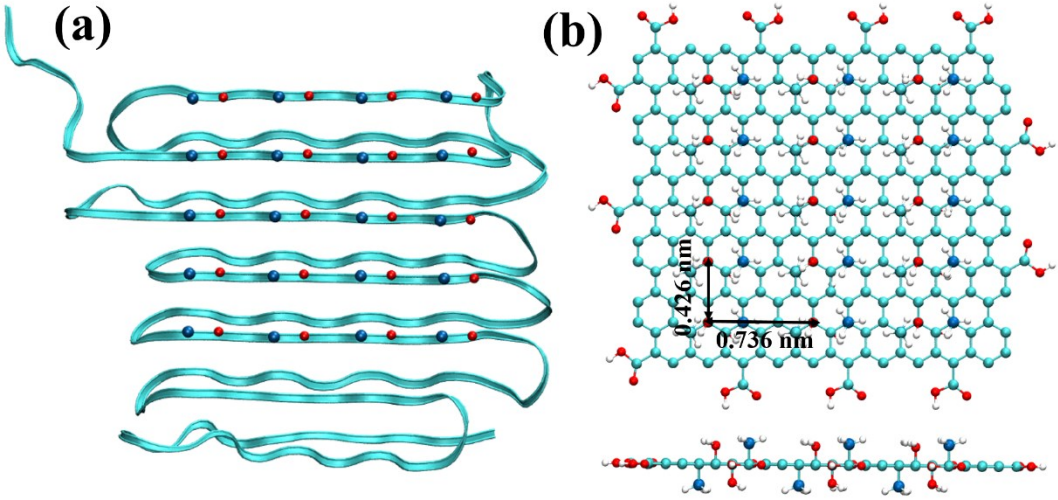

Figure S1 (a) Ice-binding sites (IBS) of hyperactive insect AFPs *Rhagium inquisitor* (RiAFP), the methyl and hydroxyl groups of the IBS are shown with light blue and red balls, respectively, and the protein backbone is shown as a cyan ribbon. (b) Top and side view of the biomimetic derivative GR–CH_3–OH–Mimic, the atoms were colored as follows: C, cyan; O, red; H, white; the carbon atom of CH_3 was colored as light blue for clarities.

As shown in Figure S2,we referred to previous work[1] to modify the hydroxyl and epoxy groups on the basal plane of graphene with randomly distribution to build the model of GR–OH–O–R. We replaced the epoxy (–O–) groups of GR–OH–O–R with amine (–NH_2) to build the model of GR–NH_2–OH–R. The similar way was used to build the model of GR–COOH–R.

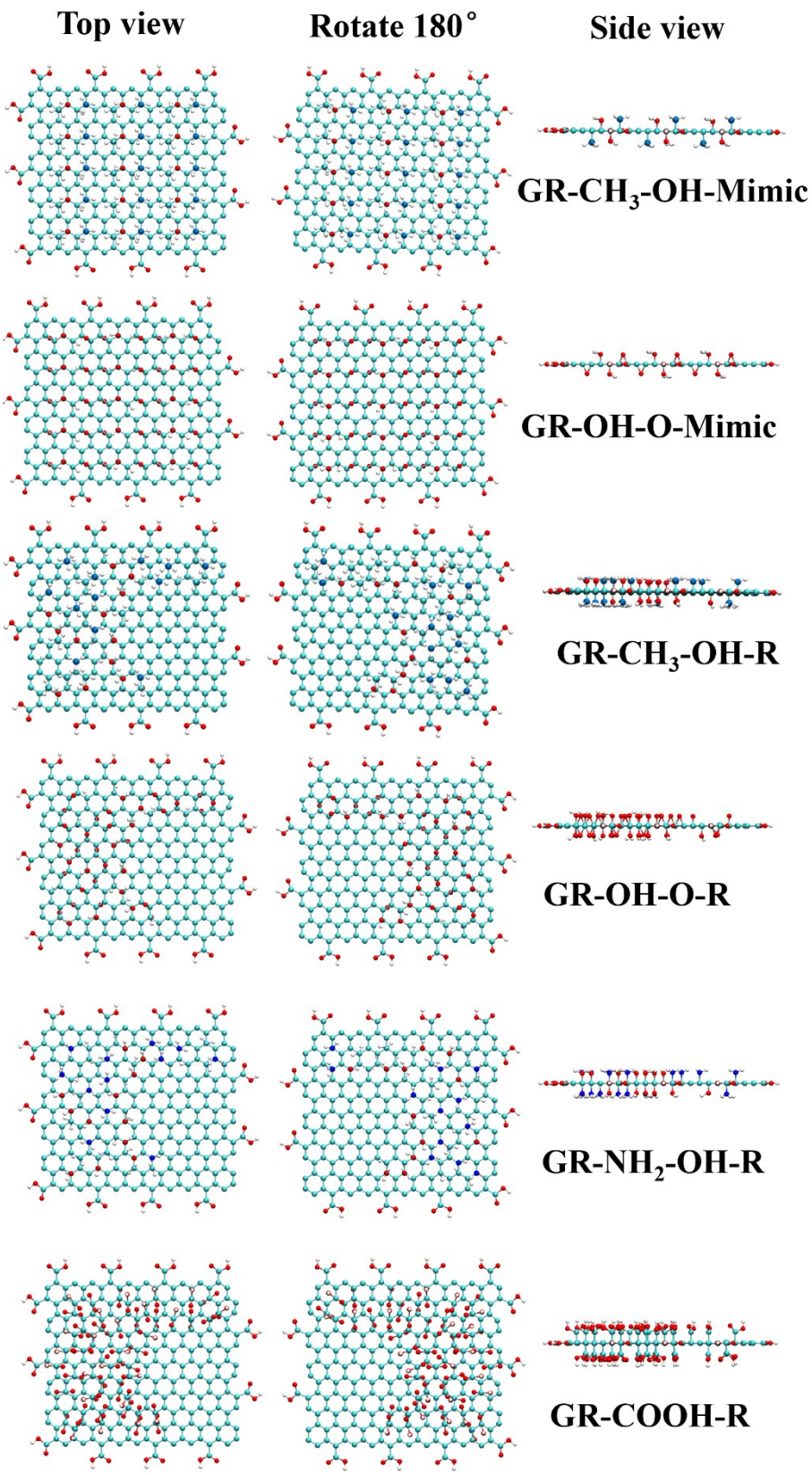

Figure S2 Top and side view of functional-group-modified graphene derivatives in our simulation calculations. The atoms were colored as follows: C, cyan; O, red; H, white; N, blue, C atom of methyl was colored as light blue for clarity.

PS2. Autocorrelation function of hydrogen bonds between the hydroxyl on the two sides of GR–CH_3–OH–Mimic and ice or water

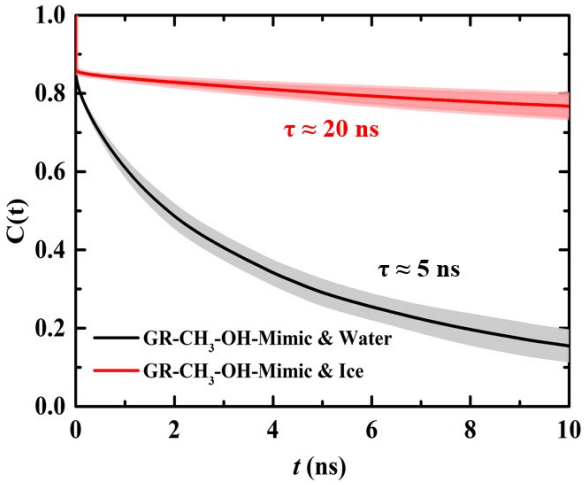

Figure S3 Autocorrelation function of hydrogen bonds between the hydroxyl on the two sides of GR–CH_3–OH–Mimic and ice or water

We adopted a commonly used geometry definition to determine if the hydrogen bonds are formed. The hydrogen bond between water molecule and oxidized groups on the basal plane were formed when the O-O distance was less than 0.35 nm and simultaneously the angle H-O···O was less than 30°.

The hydrogen bond lifetime was characterized by the autocorrelation function of hydrogen bonds,[2, 3] $C(t) = \langle h(0)h(t)\rangle / h(0)h(0)$, where h (t) =1 if the tagged molecular pair formed hydrogen bonds at time zero and still formed hydrogen bond at interval time t, otherwise h (t) = 0. The slower decay of autocorrelation function indicates the longer lifetime of hydrogen bonds. The lifetime of hydrogen bonds was obtained by fitting the exchange autocorrelation function with the exponential function $C(t) = y + A \times exp(-x/\tau)$ at the time interval form 10 ps to 10 ns, where τ was regarded as the lifetime of hydrogen bond.

PS3. Distribution of the tetrahedral order parameter $P(q_t)$ for trapped water molecules on both sides of GR–CH_3–OH–Mimic

The tetrahedral order parameter q_t was defined as $q_t = 1 - \frac{3}{32}\sum_{j<k}^{6}\left(cos\theta_{jik} + \frac{1}{3}\right)^2$ where the

sum is over all angle θ_{jik} formed around a reference molecule i by its four neareast potentional hydrogen-bonding neighbors.[4]

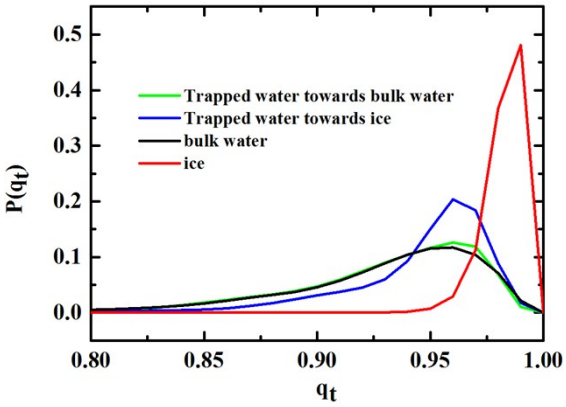

Figure S4. Distribution of the tetrahedral order parameter, P(qt) for trapped water molecules that are present within 3.2 Å from the non-hydrogen atoms of the surfaces on both sides of GR–CH_3–OH–Mimic. Corresponding distributions for pure bulk water and bulk ice are included for comparison.

PS4. Radial distribution function of water molecules on two sides of GR–CH_3–OH–Mimic.

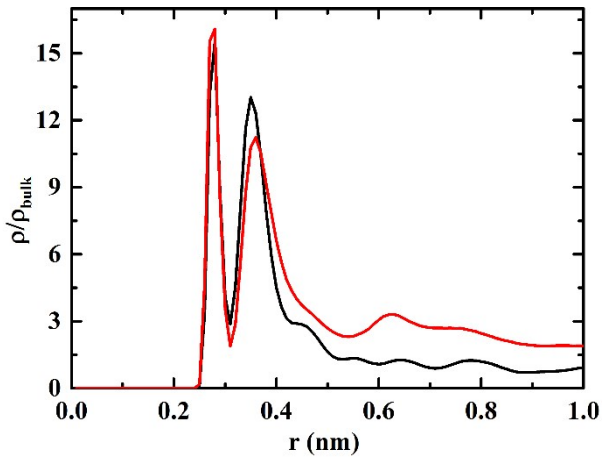

Figure S5 Radial distribution function (RDF) of water molecules on two sides of GR–CH_3–OH–Mimic. The red line represent the RDF of water molecules close to bulk water and the black line represent the RDF of water molecules close to ice, r is the distance between and oxygen atom of water molecule and function groups on two sides of GR–CH_3–OH–Mimic.

According to the radial distribution function of water molecules around the functional groups on two sides of GR–CH_3–OH–Mimic, we found that there was a clear peak at ~0.28 nm and valley at ~0.31 nm; thus we defined the first hydration layer water (r < 0.31 nm) as trapped water molecules.

PS5. Growth rate of ice crystals in different systems from theoretical calculations

We use the same method referred as the previous work[5] to determine if a water molecule belongs to ice or liquid water phase, according to the averaged hydrogen bonds number over the period of 20 ps. The geometric definition was used that two water molecular formed hydrogen bond (H-bond) if the O-O distance was less than 0.35 nm and simultaneously the angle H-O---O was less than 15°, the angle is smaller than the common used 30° to distinguish ice and water. Water molecule is in ice phase if the averaged H-bond number over the period of 20 ps was larger than 3.5, if the averaged H-bond number was smaller than 3.5, water molecule is in liquid water. The probability distribution of average H-bond number in Figure S5 shows that this method can efficiently distinguish the ice and liquid water.

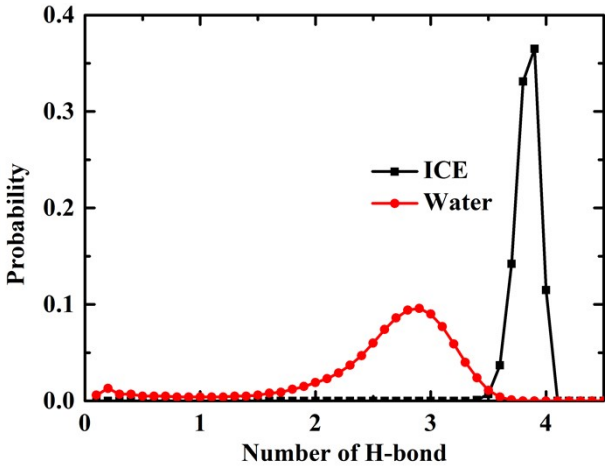

Figure S6 Probability distribution of average H-bond number for water molecule belongs to liquid water or ice phase. The red line represents the water molecule belongs to liquid water and the black line represent the water molecule belongs to ice phase.

In our simulation systems, different functional-group-modified graphene models were placed on the top of pre-formed ice crystal with the initial distance of 6 Å. During the first 10 ns, the number of water molecules forming ice was hardly affected by the functional-group-modified graphene models, after ~10 ns, the newly formed ice gradually contact with the different models, then the growth of ice crystal was affected. Thus we estimated the ice growth

rate by linear fitting the number of water molecules formed ice from 10 ns to 400 ns, the slope was the ice growth rate in different systems.

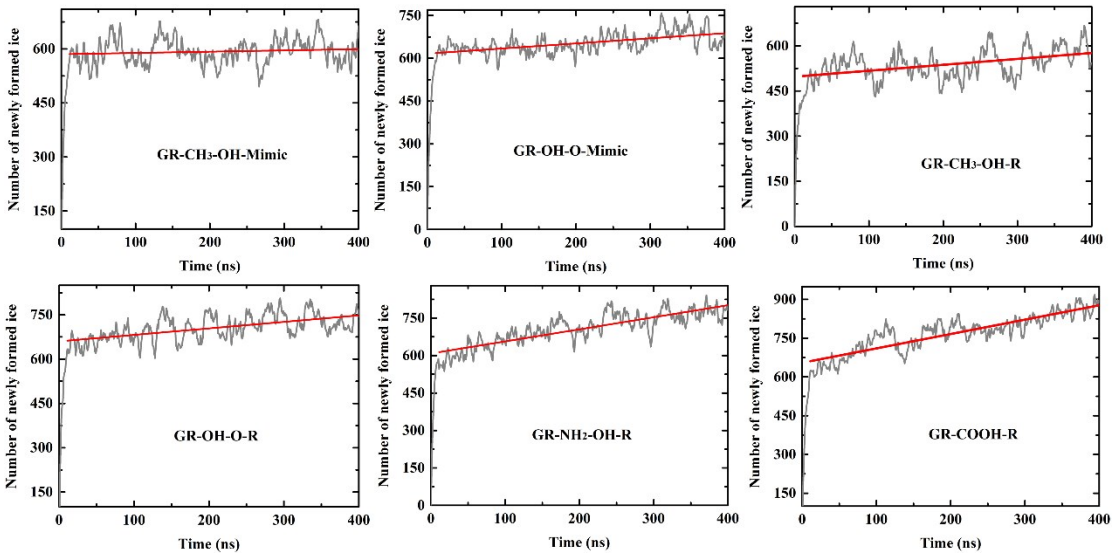

Figure S7 Number of water molecules formed ice changed with the simulation time in different systems. The red line is the linear fitting of data.

PS6. The method to calculate lifetime of trapped water molecules and dynamic properties of hydration water on the two sides of GR–CH_3–OH–Mimic

The lifetime of trapped water molecules was obtained by fitting the exchange autocorrelation function with the exponential function $C_{ex}(t) = y + A \times exp(-x/\tau)$ at the interval time from 10 ps to 10 ns, where τ was regarded as the lifetime of the trapped water.

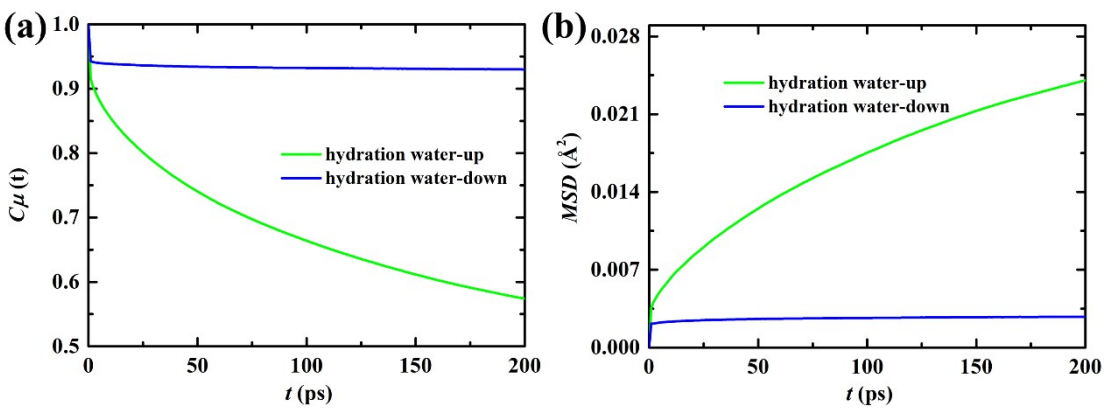

Figure S8 Dynamic properties of hydration water on the two sides of GR–CH_3–OH–Mimic. (a)

Dipole autocorrelation function of the hydration water on two sides of GR–CH_3–OH–Mimic. The data on the side close to the ice was labeled as hydration water–down and those on the side close to the bulk water was labelled as hydration water–up. (b) Mean-square displacement (MSD) of the hydration water on the two sides of GR–CH_3–OH–Mimic.

We further investigated the water dynamic properties of the hydration water that located within the second valley of the radial distribution function of water molecules around the functional group of GR–CH_3–OH–Mimic. From the literature,[4] the mean-square displacement (MSD) and autocorrelation function of water dipole $C\mu$(t) were calculated to represent the translational and reorientation dynamic properties of the hydration water on the two sides of GR–CH_3–OH–Mimic, respectively.

$$MSD = \sum_{i \in area} \left|\vec{r}_i(t) - \vec{r}_i(0)\right|^2 / N \qquad \text{(S1)}$$

where N is the total number of water molecules present in the hydration layer of GR–CH_3–OH–Mimic from $t = 0$ to interval time t all the time; note that once the water molecules moved away from the area, their movement does not contribute to the *MSD*. $\vec{r}_i(t)$ is the position of the i-th water molecule at interval time *t*, $\vec{r}_i(0)$ is the reference position of the i-th water molecule at $t = 0$.

$$C_\mu(t) = \langle \mu(t)\mu(0) \rangle / \langle \mu(0)\mu(0) \rangle \qquad \text{(S2)}$$

where μ(t) is the water dipole orientation at interval time t and the angle brackets denote averaging over water molecules.

Figure S8 (a) and Figure S8 (b) show that the autocorrelation function of the hydration water dipole close to the ice decayed slower than that close to bulk water and the MSD of the hydration water close to the ice was smaller than that close to the bulk water, which indicates that the reorientational and translational dynamics of the hydration water close to the ice are considerably slower than those close to the bulk water. The ordered stable trapped water and slow dynamic properties of hydration water close to the ice make the stable adsorption of GR–CH_3–OH–Mimic on the ice crystal. Meanwhile, the unstable exchangeable trapped water and relatively fast dynamics of the hydration water close to the bulk water cannot promote the further growth of the ice crystal. In general, AFP exhibits inhibition of ice growth through the different functional group distributions and different water structure and dynamic properties on the IBF and NIBF.[4, 6-12] Here, we integrated the different water properties into a simple two-dimensional nanomaterial, through the novel design of biomimetic model. This biomimetic model has the same functional groups with the same orderly distribution on both sides of

graphene, but it exhibits the different properties when in contact with ice or water. The ordered stable trapped water connects the GR–CH_3–OH–Mimic and ice through hydrogen bonds and the slow dynamic properties of the hydration water close to ice facilitate the stable adsorption of this biomimetic model on the ice crystal, thus suppressing the growth of the ice crystal. Meanwhile, the frequency exchanged trapped water and the faster dynamic properties of the hydration water close to the bulk water cannot be regarded as the stable ice nucleus, resulting to suppress the further nucleation and growth of the ice crystal.

PS7. The effect of GR–NH_2–OH–Mimic on ice growth

We also have built the GR–NH_2–OH–Mimic model (Figure S10) to study how it affect ice growth. The results showed that GR–NH_2–OH–Mimic was stably adsorbed on the ice crystal and the suppression of ice growth is better than the GR–NH_2–OH–R, which is in agreement with our results that the ordered functional group distribution on graphene matching the ice crystal lattice is important for stable adsorption to suppress ice growth.

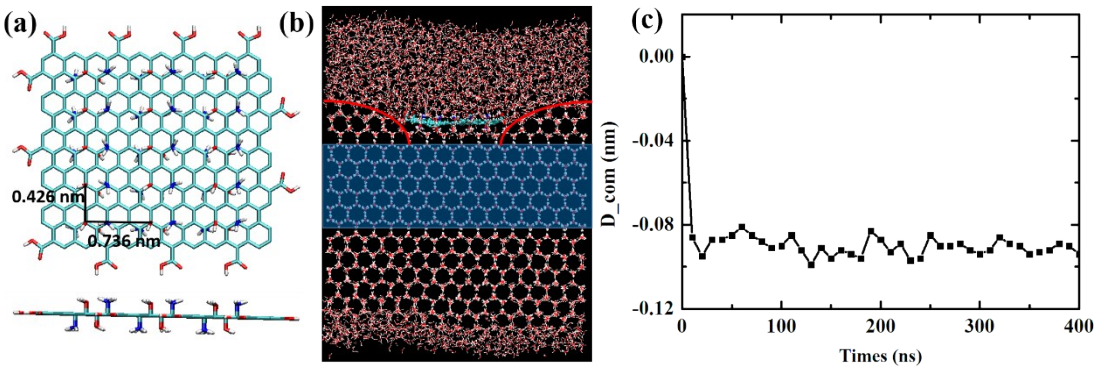

Figure S9 (a) Top and side view of the GR–NH_2–OH–Mimic: C, cyan; O, red; H, white; N, blue. (b) MD simulation snapshot of the GR–NH_2–OH–Mimic adsorption on the ice crystal at 400 ns: the pre-formed ice crystal is covered by light blue, and water is shown in red lines. (c) Center of mass displacement of GR–NH_2–OH–Mimic along the z-axis with the simulation time.

PS8. The snapshot of trapped water molecules on two sides of GR–OH–O–Mimic

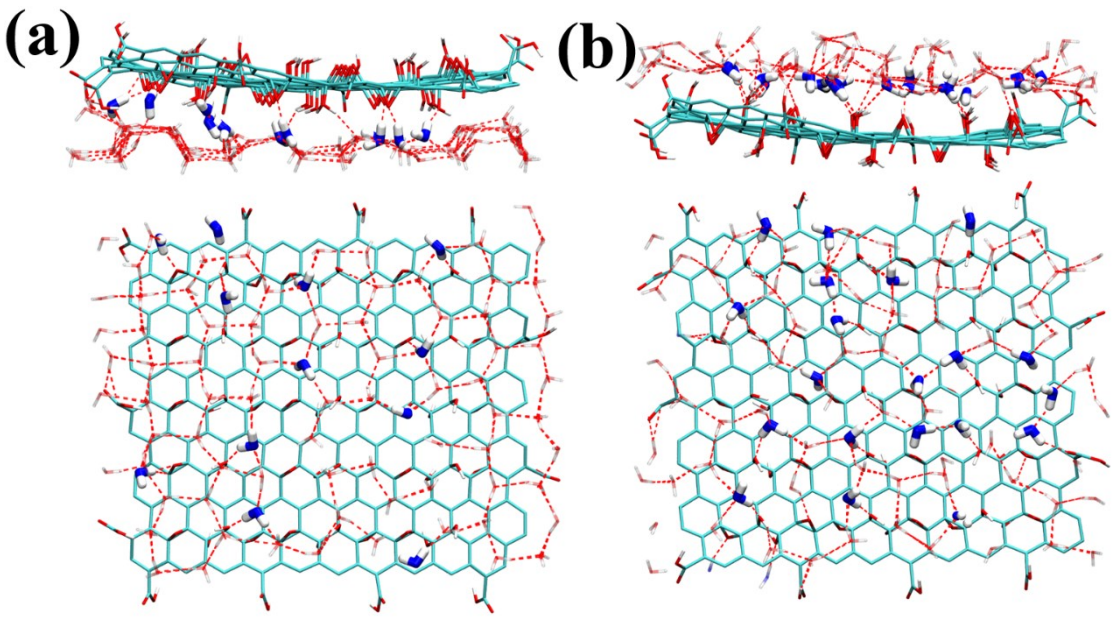

Figure S10 Typical snapshot of water molecules around GR–OH–O–Mimic close to the ice (a) and the bulk water (b) respectively. C, cyan; O, red; H, white; hydrogen bonds, red dashed lines; the oxygen of trapped water was colored as blue for clarities.

PS9. Details of experimental growth rates of ice crystals in the presence of different functional group modified graphene

Nanoliter osmometer experiments: The growth of single ice crystals at various supercooling temperatures was monitored by an optical microscope through an Otago Nanoliter Osmometer (Otago Osmometers Ltd., Dunedin, New Zealand) with a precision of 0.01 °C. The temperature controller chamber was dehydrated with dry purified nitrogen (99.99%, 25 °C). All the testing procedures followed study reported elsewhere.[1, 13] First, the system was calibrated using ultrapure water and 0.05 mol kg^{-1} NaCl solution to obtain the 'zero' and '– 0.18 °C' points, respectively. Afterwards, sub-microliter volume of the different functional group modified graphene derivatives (GR–OH–O–R, GR–NH_2–OH–R, GR–COOH–R) dispersion were injected into a temperature-controlled sample holder full of silicone oil using a microsyringe with the tip connected to a glass capillary. The droplet of the different functional group modified graphene derivatives (GR–OH–O–R, GR–NH_2–OH–R, GR–COOH–R) dispersion immerged in oil was quickly frozen then slowly warmed to its melting temperature. A number of ice crystals will form at this melting temperature. Once a small (~15–20 μm in diameter) single ice crystal appeared, the temperature is slightly tuned to keep the single ice crystal for at least 20 s. This temperature was recorded as the melting temperature (T_m). Then the temperature was decreased to a desired value (T_f). Supercooling temperature (ΔT) is obtained by subtracting T_f

from T_m. The experiment was repeated at least three times for each ΔT. The growth of ice crystals was recorded by a high-speed camera (Phantom V7.3). The growth rate was determined from the recorded images via dividing the elongation by the time elapsed during the growth course, and a mean value was calculated from the repeated experimental videos. T tests were performed to 95% confidence level. The ΔT at which the ice crystal bursts suddenly are deemed to the TH gap of the test sample.

References

(1) Geng, H.; Liu, X.; Shi, G.; Bai, G.; Ma, J.; Chen, J.; Wu, Z.; Song, Y.; Fang, H.; Wang, J., Graphene Oxide Restricts Growth and Recrystallization of Ice Crystals. *Angew. Chem. Int. Ed.* **2017,** *56*, 997-1001.

(2) Balasubramanian, S.; Pal, S.; Bagchi, B., Hydrogen-Bond Dynamics near a Micellar Surface: Origin of the Universal Slow Relaxation at Complex Aqueous Interfaces. *Phys. Rev. Lett.* **2002,** *89*, 115505.

(3) Pal, S.; Balasubramanian, S.; Bagchi, B., Dynamics of Bound and Free Water in an Aqueous Micellar Solution: Analysis of the Lifetime and Vibrational Frequencies of Hydrogen Bonds at a Complex Interface. *Phys. Rev. E* **2003,** *67*, 061502.

(4) Nutt, D. R.; Smith, J. C., Dual Function of the Hydration Layer around an Antifreeze Protein Revealed by Atomistic Molecular Dynamics Simulations. *J. Am. Chem. Soc.* **2008,** *130*, 13066-13073.

(5) Carignano, M.; Shepson, P.; Szleifer*, I., Molecular Dynamics Simulations of Ice Growth from Supercooled Water. *Mol. Phys.* **2005,** *103*, 2957-2967.

(6) Liou, Y.-C.; Tocilj, A.; Davies, P. L.; Jia, Z., Mimicry of Ice Structure by Surface Hydroxyls and Water of a B-Helix Antifreeze Protein. *Nature* **2000,** *406*, 322-324.

(7) Meister, K.; Strazdaite, S.; DeVries, A. L.; Lotze, S.; Olijve, L. L.; Voets, I. K.; Bakker, H. J., Observation of Ice-Like Water Layers at an Aqueous Protein Surface. *Proc. Natl. Acad. Sci.* **2014,** *111*, 17732-17736.

(8) Liu, K.; Wang, C.; Ma, J.; Shi, G.; Yao, X.; Fang, H.; Song, Y.; Wang, J., Janus Effect of Antifreeze Proteins on Ice Nucleation. *Proc. Natl. Acad. Sci..* **2016,** *113*, 14739-14744.

(9) Hudait, A.; Odendahl, N.; Qiu, Y.; Paesani, F.; Molinero, V., Ice-Nucleating and Antifreeze Proteins Recognize Ice through a Diversity of Anchored Clathrate and Ice-Like Motifs. *J. Am. Chem. Soc.* **2018,** *140*, 4905-4912.

(10) Hudait, A.; Qiu, Y.; Odendahl, N.; Molinero, V., Hydrogen-Bonding and Hydrophobic Groups Contribute Equally to the Binding of Hyperactive Antifreeze and Ice-Nucleating Proteins to Ice. *J. Am. Chem. Soc.* **2019,** *141*, 7887-7898.

(11) Chakraborty, S.; Jana, B., Molecular Insight into the Adsorption of Spruce Budworm Antifreeze Protein to an Ice Surface: A Clathrate-Mediated Recognition Mechanism. *Langmuir* **2017,** *33*, 7202-7214.

(12) Midya, U. S.; Bandyopadhyay, S., Interfacial Water Arrangement in the Ice-Bound State of an Antifreeze Protein: A Molecular Dynamics Simulation Study. *Langmuir* **2017,** *33*, 5499-5510.

(13) Bai, G.; Song, Z.; Geng, H.; Gao, D.; Liu, K.; Wu, S.; Rao, W.; Guo, L.; Wang, J., Oxidized Quasi-Carbon Nitride Quantum Dots Inhibit Ice Growth. *Adv. Mater.* **2017,** *29*, 1606843.